Journal Title
XX(X):1–17

DOI: 10.1177/ToBeAssigned
www.sagepub.com/
SAGE

A variable admittance control strategy for stable physical human-robot interaction

Federica Ferraguti[1], Chiara Talignani Landi[1], Lorenzo Sabattini[1], Marcello Bonfè[2], Cesare Fantuzzi[1] and Cristian Secchi[1]

Abstract

Admittance control allows to reproduce a desired dynamic behavior on a non-backdrivable manipulator and it has been widely used for interaction control and, in particular, for human-robot collaboration. Nevertheless, stability problems arise when the environment (e.g. the human) the robot is interacting with gets too stiff. In this paper, we investigate the stability issues related to a change of stiffness of the human arm during the interaction with an admittance-controlled robot. We propose a novel method for detecting the rise of instability and a passivity preserving strategy for restoring a stable behavior. The results of the paper are validated on two robotic setups and with 50 users performing two tasks that emulate industrial operations.

Keywords

physical human-robot interaction, cooperative manipulators, admittance control, human-in-the-loop

1 Introduction

In the last few years, a growing attention on physical human-robot interaction (pHRI) and collaborative robotics has allowed to leave behind the old paradigm of robots working inside safety cages, converting them into collaborators that work side by side with humans. Different tasks can be accomplished with robots, like assisted industrial manipulation, collaborative assembly, domestic work, entertainment, rehabilitation or medical applications. Due to this tight cooperation and coexistence of humans and robots sharing the same workspace, safety and dependability are of paramount importance.

Different approaches have been developed to implement a reliable pHRI, exploiting control strategies that make the robot compliant (see, e.g., Villani and De Schutter (2008)). In the industrial scenario, the admittance control is particularly appealing since it allows to exploit existing industrial, non-backdrivable, manipulators. For example, admittance control has been used to implement robot manual guidance in Talignani Landi et al. (2016) and Ferraguti et al. (2017), by means of the "walk-through programming" where the human operator becomes the teacher that physically guides the robot throughout the desired trajectory.

When using admittance-controlled robots, instability can arise when interacting with stiff environments. This can be due to several factors as the robot structural dynamics, the actuators limitations and the low-level controllers implementations (Eppinger and Seering (1986)). All these destabilizing effects are due to the violation of the co-location principle, as shown in Colgate and Hogan (1989).

Since humans are dynamic systems characterized by a time-varying impedance, they can behave in a stiff way and, consequently, give rise to instability when interacting with admittance-controlled robot. In Tsumugiwa et al. (2004) it is shown that this effect, combined with the time delay in the human reaction and the compliance in the robot structure, can cause instabilities during a cooperative transportation task. As shown in Peer and Buss (2008), instability is related to the human arm impedance, especially when the user grasps the tool placed on the end-effector in a very stiff way. Moreover, it is always possible to choose an admittance dynamics that makes the human-robot system unstable (Peer and Buss (2008)).

Instability induces, among other undesired effects, a deviation of the robot from the desired admittance behavior. Furthermore, it produces high amplitude oscillations of the end-effector, undermining the user safety during the interaction. Thus, it is very important to promptly detect the rise of oscillations and then act for restoring a stable and safe behavior.

An effective method for recovering stability consists in modifying the admittance dynamics parameters. The most common strategy consists in increasing the desired damping of the admittance. This action increases the dissipation of the system and restores a passive and stable behavior. Nevertheless, a bigger damping factor affects the admittance dynamics and requires a larger effort for the human in the interaction with the robot (Dimeas and Aspragathos (2016)). Moreover, changing only one of the parameters completely unbalances the admittance dynamics, and this tremendously affects the usability of the robot (Lecours et al. (2012)).

[1]Department of Science and Methods for Engineering, University of Modena and Reggio Emilia, Italy
[2]Engineering Department, University of Ferrara, Italy

Corresponding author:
Federica Ferraguti, Department of Science and Methods for Engineering, University of Modena and Reggio Emilia, via Amendola 2, 42122 Reggio Emilia, Italy.
Email: federica.ferraguti@unimore.it

In this paper we propose a novel methodology for detecting the rise of oscillations during the interaction between a human and an admittance-controlled robot and a passivity based parametric adaptation of the admittance for restoring a stable behavior. The proposed adaptation allows to keep the adaptive dynamics similar to the nominal one in order to avoid unbalancing effects and to increase the usability of the system.

Preliminary results have been presented in Talignani Landi et al. (2017b) and Talignani Landi et al. (2017a). In this paper we present the following significant extensions:

- The heuristic for detecting instability proposed in Talignani Landi et al. (2017b) and Talignani Landi et al. (2017a) was based on an empirically chosen threshold. In this work we propose a new methodology for automatically setting the detection threshold using a thorough statistical analysis.
- The passivity based parametric adaptation proposed in Talignani Landi et al. (2017b) and Talignani Landi et al. (2017a) leads to a conservative approach since it treats all the degrees of freedom (DOFs) in the same way. In this paper, we overcome this limit adding a weighted energy allocation strategy in order to consider separately translations and rotations.
- We provide an extended experimental validation with a larger number of users and two robots (a Puma 260 and a KUKA LWR 4+) to demonstrate that the presented algorithm is hardware independent and user adaptive, without the need of an initial profiling of the human operator. Moreover, we provide an experimental comparison with state-of-the-art methods that address the detection and handling of instability in admittance control.

The remainder of this paper is organized as follows: in Section 2, a comparison between our method and related works is presented. Section 3 gives background information on the admittance control and the main issues in Human-Robot Interaction, while, in Section 4, the procedure to detect online the rising oscillations is described. Section 5 shows the methodology for parameter adaptation with weighted energy allocation. In Section 6, we describe the experiments carried out with two different robotic setups, where the objective was to perform a precision and a velocity task; subsequently, we show the results of the experimental comparison of the proposed method with state-of-the-art approaches. Finally, in Section 7, a discussion of the results is proposed and the conclusions are drawn.

2 Related Works

Different approaches are available in the literature to overcome rising instabilities during the pHRI in response to a high human arm stiffness. A first method consists in estimating the arm stiffness and adapting the controller parameters consequently. In Tsumugiwa et al. (2002) the authors propose to increase the damping coefficient proportionally to the estimated stiffness of the human arm, in order to stabilize the system. However, the user physical effort is increased and a dynamic model of the arm is needed. In Duchaine and Gosselin (2008), authors first estimate the human arm stiffness with recursive experiments, then they find the Lyapunov function for the closed loop system that allows to define the stability frontiers and the critical value of each impedance parameter. In particular they fix the mass to the value that makes the system critically stable, and they find the critical damping experimentally. In this case, the impedance parameters are fixed and cannot be changed during the task execution, and the stiffness estimation has to be done each time the user changes.

Another approach exploits electromyography (EMG) sensors to evaluate when the user is stiffening his/her arm. For example, in Gallagher et al. (2014), the information provided by the EMG sensor is used to estimate the muscle activity and, consequently, the user stiffness, adjusting the impedance controller parameters. In particular, the initial damping value is increased along with the user stiffness to counteract the oscillations and to allow the haptic device to be held steadily. The work in Grafakos et al. (2016) presents a variable admittance control where the damping parameter is adjusted between two predefined values when the EMG sensors detect a co-contraction in the operator's arm muscles. In both cases only the damping increased, which requires larger human physical effort and additional sensors.

An example of an external device that helps in stabilizing the system is presented in Lamy et al. (2009): the designed handle, coated with foam that acts as a mechanical filter, is mounted on the robot end-effector and it is used to estimate the human grasping force during a co-manipulation task. The parameters in the designed PI robot controller are changed accordingly to the performed estimation.

Other approaches, not requiring external devices or additional sensors, are based only on interaction force and end-effector position measurements. For example, in Erden and Marić (2011), a method is presented that computes the variance of the measured tool positions during the performance phase of a welding task. This criterion takes into account the oscillations of the torch: the smaller is the variance, the more successful is the welding. Hence, a proper high damping value is determined, to obtain an effective vibration suppression during the welding, while a low value is set during the movement of the torch from one point to another. They proved that this method helps untrained users, but they only switch between two damping values that are set a priori for all of the operators, excluding the possibility of tuning the parameters according to different users. In Podobnik and Munih (2007), the contact instability of the admittance control of a haptic interface is investigated. The human grasping force is measured and its critical value that destabilizes the system is determined. To improve stability two methods are applied: the first one exploits the virtual coupling (i.e. an artificial link between the haptic display and a virtual environment); the second one features a compensator used as a filter of the input force exerted by the human operator. In Duchaine et al. (2012), a method is proposed to estimate the interaction stiffness exploiting the force/torque sensor used for the admittance control. As a consequence, a stability observer is defined that detects oscillations and adapts the damping matrix in real time.

Approaches based on the frequency analysis of a signal (i.e. force, velocity or position) are presented in Dimeas

and Aspragathos (2016), Ryu et al. (2008), and Okunev et al. (2012). In Dimeas and Aspragathos (2016), a stability observer is proposed, based on the frequency analysis of the force signal generated from the interaction between the operator and the robot. Consequently, an instability index is built and the admittance parameters (i.e. inertia and damping) are proportionally increased. In Ryu et al. (2008), a haptic stability observer examines the motion in the frequency domain and quantifies the degree of instability. Hence a damping force is generated by the controller to counteract the oscillations. A frequency analysis is done also in Okunev et al. (2012), where the fast Fourier transform (FFT) of the measured forces at the end-effector, in combination with boosted classifiers, allows to detect instability oscillations and modify the admittance control parameters consequently. The carried out simulations show that the primary method to avoid oscillations consists in increasing the inertia. Nevertheless, the frequency analysis introduces a delay in the compensation that can reduce its effectiveness.

The time-domain vibration observer presented in Campeau-Lecours et al. (2016) addresses the interaction stability issue by means of an adaptive control strategy. A vibration index is computed and then used to adjust the control gains in order to reduce the vibrations that appear when the operator grasps the end-effector in a stiff manner. Different control strategies are possible: the admittance control parameters (i.e. inertia and damping) can be linearly varied between two values, a damping can be added, or the low-level controller gains can be reduced. A common strategy, based on energy flow, that allows to control a haptic system ensuring stable contact is the passivity observer (PO) and passivity controller (PC) implementation (Hannaford and Ryu (2002)). Nevertheless, as highlighted in Campeau-Lecours et al. (2016), the use of PO-PC during the interaction with a stiff user does not detect any instability oscillation. Indeed, in the PO output the energy does not become negative: the passivity controller would apply corrections only when extra energy is injected into the system in response to an active behavior, but it would not apply any correction when the vibrations are due to a stiff but passive environment.

Unlike the presented approaches, our work aims at proposing a methodology for detecting the rising oscillations in pHRI that is independent from the velocity and acceleration bounds of the robot and does not require external devices or frequency analysis computations. Furthermore, the proposed parameter adaptation strategy allows to restore stability while preserving a passive behavior of the admittance dynamics. This is very important because changing parameters of a (virtual) physical dynamics can lead to a non passive and, therefore, unstable dynamics. Thus, if passivity is not guaranteed, it may happen that the stabilizing mechanism (i.e. changing parameters) induces instability because of a loss of passivity.

3 Background on admittance control and issues in human-robot interaction

Consider a n-degree of freedom (n-DOF) manipulator controlled by using the admittance control scheme shown in Fig. 1. Given a desired interaction model, namely a dynamic relation between the motion of the robot and the force applied by the environment, and given the external force, the admittance equation, via a suitable integration (see, e.g., De Stefano et al. (2017b,a) for explicit passive integration strategies), generates the position and orientation to be used as a reference for a low-level position controller. The goal of the admittance control is to force the robot to behave compliantly with the environment, according to a given mass-spring-damper system. The elastic part of this system is used to attract the robot end-effector towards a desired pose. However, since we want to address the case of a robotic manipulator manually driven by the human operator, in this paper we do not consider the elastic part of the general admittance control model (Villani and De Schutter (2008)). Indeed, the user guides the robot by means of the force applied to its end-effector, without directly specifying a desired pose. Let $\bar{x}(t) \in \mathbb{R}^6$ be the set-point computed by the admittance controller and $x(t) \in \mathbb{R}^6$ be the pose of the end-effector, obtained from the joint positions $q(t) \in \mathbb{R}^m$, $m \geq 6$, through the forward kinematics. For ease of notation we will hereafter omit the dependency of $q(t)$ from t. We expect that the low-level position controller is designed and tuned to minimize the tracking error and optimize the dynamic response so that the robot can track a feasible set-point. Thus, we will make the following assumption:

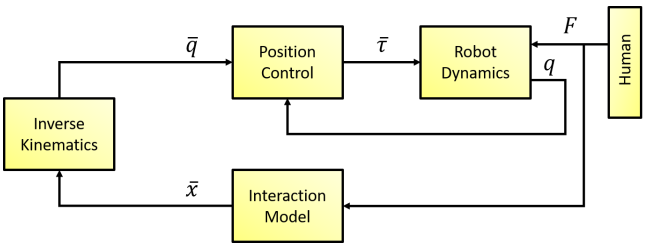

Figure 1. Control scheme of the admittance control with underlying motion controller. The solution of the interaction model with the input $F(t)$ provides the value $\bar{x}$ which the position-controlled robot must follow, by computing the desired joint positions $\bar{q}$ from inverse kinematics and regulating the joint torque τ to let the actual joint positions q track $\bar{q}$.

Assumption 1. *The low-level position controller is designed and tuned in such a way that $x(t) \simeq \bar{x}(t)$ as long as*

$$\begin{aligned} -\dot{\mathcal{X}}(q) \leq \dot{\bar{x}}(t) \leq \dot{\mathcal{X}}(q) \\ -\ddot{\mathcal{X}}(q) \leq \ddot{\bar{x}}(t) \leq \ddot{\mathcal{X}}(q) \end{aligned} \tag{1}$$

where

$$\begin{aligned} \dot{\mathcal{X}}(q) = \left[\dot{\mathcal{X}}_1, \ldots, \dot{\mathcal{X}}_6\right]^T \in \mathbb{R}^6 \\ \ddot{\mathcal{X}}(q) = \left[\ddot{\mathcal{X}}_1, \ldots, \ddot{\mathcal{X}}_6\right]^T \in \mathbb{R}^6 \end{aligned} \tag{2}$$

are configuration-dependent velocity and acceleration bounds due to the robot dynamics and the inequalities are component-wise.

We want to force the robot to interact with the environment according to the following desired behavior:

$$M_d \ddot{x}(t) + D_d \dot{x}(t) = F(t) \tag{3}$$

where $M_d \in \mathbb{R}^{6\times6}$ and $D_d \in \mathbb{R}^{6\times6}$ are the desired inertia and damping symmetric and positive definite matrices. The

external force $F(t) \in \mathbb{R}^6$ in (3) is assumed to be measured by a 6-DOF force/torque (F/T) sensor attached at the robot wrist flange. The controlled robot behaves as (3) and it is passive with respect to the pair $(F(t), \dot{x}(t))$, as proved in Ferraguti et al. (2015).

During the execution of the cooperative task, the robot is coupled with a human operator, whose dynamics (e.g. change of compliance of the arm) can cause deviations from the desired behavior that may produce robot oscillating motions of high amplitude and frequency, making the interaction unsafe for the user (Dimeas and Aspragathos (2016)). Thus, the oscillations have to be detected and then the desired behavior has to be recovered.

A common strategy for restoring the desired behavior of the controlled robot in the presence of deviation is to adapt the parameters of the admittance control (see, e.g., Ranatunga et al. (2017)). As shown in Dimeas and Aspragathos (2016), three different adaptation laws can be used to stabilize the system: increase the damping, increase the inertia or increase both the damping and the inertia while keeping a constant ratio. Thus, in order to be able to compensate the destabilizing effects by adapting the parameters, we implement the following, time-varying, interaction model:

$$M(t)\ddot{x}(t) + D(t)\dot{x}(t) = F(t) \tag{4}$$

where $M(t) \in \mathbb{R}^{6\times6}$ and $D(t) \in \mathbb{R}^{6\times6}$ are inertia and damping symmetric and positive definite matrices such that $M(0) = M_d$ and $D(0) = D_d$. While increasing the damping is an intuitive and passivity preserving approach since it increases the energy dissipated, changing the inertia is, in general, a non passive operation (Ferraguti et al. (2015)). Thus, it may happen that the procedure for stabilizing the interaction makes the admittance dynamics non passive and possibly unstable. Nevertheless, using the method explained in the following sections, it is possible to adapt both the damping and inertia parameters in (4) while preserving the passivity of the initial dynamics.

In Talignani Landi et al. (2017b) the following simple heuristic for detecting the rise of an oscillatory behavior during the cooperation has been proposed:

$$\|F(t) - M(t)\ddot{x}(t) - D(t)\dot{x}(t)\| \leq \varepsilon \tag{5}$$

where $\varepsilon \in \mathbb{R}^+$ is an appropriately defined small threshold. When (5) is not satisfied, the robot is considered to be deviating from the interaction model imposed by the admittance control. Unfortunately, since oscillating motions have a high frequency, that corresponds to high values of velocities and accelerations, the threshold indicating such a deviation strongly depends on the maximum velocity and acceleration achievable by the robot and on the time-varying admittance parameters. This makes ε also time-varying and hard to tune. In Talignani Landi et al. (2017a) a novel condition for detecting the rise of high-frequency oscillations that is more robust than (5) has been proposed. However, the value of the detection threshold ε still has to be manually found through post-processing operations.

4 Online detection of rising oscillations in physical human-robot interaction

In order to overcome the drawbacks introduced by the use of real-time computations of (5) to detect the rising oscillations, in this section we will introduce an improved heuristic and a practical procedure for tuning the detection threshold ε.

4.1 Definition of the heuristic

Let us define the vectors $\dot{\hat{x}}(t) \in \mathbb{R}^6$ and $\ddot{\hat{x}}(t) \in \mathbb{R}^6$ as the tracking error derivatives scaled with respect to the bounds $\dot{\mathcal{X}}$ and $\ddot{\mathcal{X}}$. In particular, the j-th components of the scaled vectors are defined as follows:

$$\dot{\hat{x}}_j(t) = \frac{\dot{\tilde{x}}_j(t)}{\dot{\mathcal{X}}_j(q)} \qquad \ddot{\hat{x}}_j(t) = \frac{\ddot{\tilde{x}}_j(t)}{\ddot{\mathcal{X}}_j(q)} \qquad j = 1, \ldots, 6 \tag{6}$$

where

$$\begin{aligned} \dot{\tilde{x}}(t) &= \dot{\tilde{x}}(t) - \dot{x}(t) = \left[\dot{\tilde{x}}_1(t) \ldots \dot{\tilde{x}}_6(t)\right]^T \in \mathbb{R}^6 \\ \ddot{\tilde{x}}(t) &= \ddot{\tilde{x}}(t) - \ddot{x}(t) = \left[\ddot{\tilde{x}}_1(t) \ldots \ddot{\tilde{x}}_6(t)\right]^T \in \mathbb{R}^6 \end{aligned} \tag{7}$$

are the first and second order derivatives of the tracking error. Robot velocities and accelerations can be measured using specific hardware (e.g. gyroscopes and accelerometers) or estimated using, for example, the quaternion-based Kalman filter introduced in Farsoni et al. (2017).

Moreover, we introduce the following damping to inertia ratio matrix:

$$R_d(t) = M^{-1}(t)D(t) \tag{8}$$

We can now define the improved heuristic in terms of (6) and (8), as follows:

$$\psi\left(\dot{\hat{x}}(t), \ddot{\hat{x}}(t)\right) = \|\ddot{\hat{x}}(t) + R_d(t)\dot{\hat{x}}(t)\| \leq \varepsilon \tag{9}$$

With a slight abuse of notation, we will hereafter use $\psi(t)$ to indicate the value of $\psi\left(\dot{\hat{x}}(t), \ddot{\hat{x}}(t)\right)$ at time t. We propose to use (9) as the heuristic for detecting online when oscillations occur. Namely, when (9) is not satisfied, we claim that oscillations are rising. Unlike (5), this novel formulation of the detection index is intrinsically insensitive to the physical characteristics of the robot in use, thanks to the scaling with respect to velocity and acceleration bounds (6), and its sensitivity against the current values of inertia and damping matrices is mitigated. Indeed, (9) contains the damping to inertia ratio (8) that multiplies only the scaled velocity error, which is generally much smaller than the scaled acceleration error, in case of high-frequency oscillations.

4.2 Experimental statistical characterization of the detection index $\psi(t)$

In the last part of this section (Section 4.3) we will propose, as a novel contribution of this paper, a practical procedure to tune the detection threshold ε. The proposed procedure is based on the results of the following experimental characterization of the detection index $\psi(t)$. The characterization is based on statistical methods and on the following assumptions.

Assumption 2. *Given an initial choice of the admittance parameters M_d and D_d that is feasible for the characteristics*

of the robot (Lecours et al. (2012)) and for the desired interaction task, an experienced human operator can interact properly with the robot (i.e. without causing oscillating behaviors), applying a gentle grasp and softening his/her arm.

Assumption 2 is not restrictive in practice, provided that the chosen admittance parameters M_d and D_d are not excessively small (Lecours et al. (2012)).

Assumption 3. *The detection index $\psi(t)$ is a random variable whose Probability Density Function (PDF), and its related Cumulative Distribution Function (CDF), can be estimated from experimental data.*

Assumption 3 derives from considering that the detection index $\psi(t)$ is a function of the tracking error. Since a robotic manipulator is a complex nonlinear system subject to different sources of uncertainty (e.g. measurement and modeling errors, external disturbances, etc.), its tracking error is generally described by means of non-Gaussian stochastic models (Chen et al. (2009)).

Assumption 4. *The admittance control adaptation law (see Section 5.2) is designed to preserve a constant damping to inertia ratio.*

Assumption 4 represents a recommended practice in physical human-robot interaction (see Lecours et al. (2012)). Indeed, this choice allows to maintain a similar dynamics of the system after the adaptation, which is more intuitive for the operator rather than increasing only the inertia or only the damping. Assumption 4 implies that the threshold ε is tuned for a given initial value of the damping to inertia ratio $R_d(0)$, generally set according to the desired interaction task, and has to be re-tuned only if such a parameter setting is changed.

We performed several experiments in order to obtain the statistical characterization of the detection index $\psi(t)$. In particular, under Assumption 2, an experienced operator applied persistent inputs to $F(t)$ and forced the robot to move within a large part of its workspace, while avoiding joint limits and singular configurations and without causing oscillations. In the meanwhile, the value of $\psi(t)$ is calculated and discrete-time samples are recorded. The time series of $\psi(t)$ collected during the experiments were analyzed to search for a probability distribution properly fitting the data and thus to estimate the PDF and the related CDF.

In order to fully characterize the probability distribution of $\psi(t)$, the experiments were performed on two different robotic system (a KUKA LWR 4+ and a Puma 260) with different (experienced) users who interacted with the admittance-controlled robots and with different values of the admittance model parameters. We chose diagonal inertia and damping matrices, resulting in diagonal damping to inertia ratio matrices*. We performed the experiment with the following damping to inertia ratio on each robotic setup:

- *Test 1*: 12.5 $^{kgNs}/_{m}$ on translational DOFs and 25 $^{kgNs}/_{mrad}$ on rotational DOFs
- *Test 2*: 1.25 $^{kgNs}/_{m}$ on translational DOFs and 2.5 $^{kgNs}/_{mrad}$ on rotational DOFs

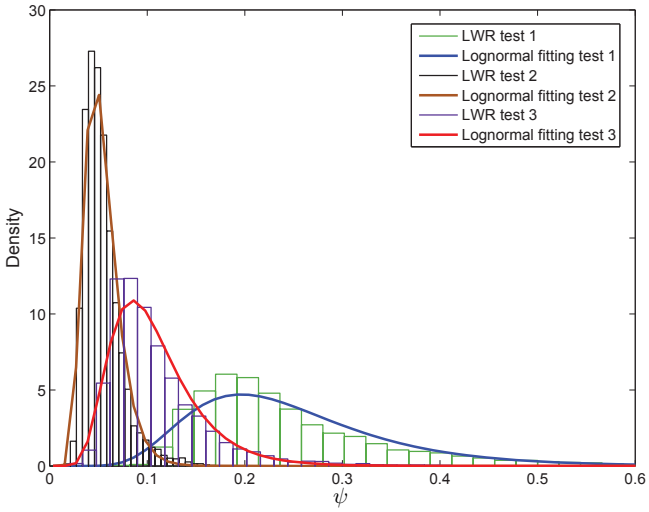

Figure 2. Histogram distributions and fitted log-normal PDFs for the experiments with the KUKA LWR 4+ robot.

- *Test 3*: 5 $^{kgNs}/_{m}$ on translational DOFs and 10 $^{kgNs}/_{mrad}$ on rotational DOFs

In order to define the PDF that best characterizes $\psi(t)$, we considered only distributions supported on the semi-infinite interval $[0, \infty)$ (e.g. Birnbaum-Saunders, Gamma, log-logistic, log-normal, Weibull, etc.) (Johnson et al. (1995)), being the values of $\psi(t)$ strictly positive by definition. As a result of this study, the log-normal distribution was selected for the statistical characterization of the detection index $\psi(t)$ because its goodness of fit was the best or the second best for all of the experiments and its parameters can be estimated with simple formulas, applying the Maximum Likelihood Estimation (MLE) method (Ginos (2009)). The plots in Figures 2 and 3 show the histogram distributions of the data acquired during the three tests with, respectively, the KUKA LWR 4+ and the Puma 260, together with the log-normal PDFs whose parameters are calculated with MLE from such data. As can be seen, the two robotic systems provide similar experimental results, being the distributions centered on higher values of $\psi(t)$ for higher damping to inertia ratios. Slight differences in the quantitative evaluations could be ascribed to the differences in the tracking performances of the low-level position controllers of the two robots. Since the different damping to inertia ratios result in similar robot behaviors, we chose the ratio of Test 1 and performed experiments in the following conditions:

- three different periods (30, 60, 120 seconds);
- three experienced users;
- two different values of inertia and damping (keeping the ratio constant according to Test 1).

In all of these cases, the estimated parameters of the log-normal distribution did not change significantly, leading to similar results in terms of PDF distribution fitting. The

*The choice of diagonal matrices is aimed at simplifying the notation for the comparison. Indeed, the desired inertia and damping matrices can be freely chosen, provided that they are symmetric and positive definite.

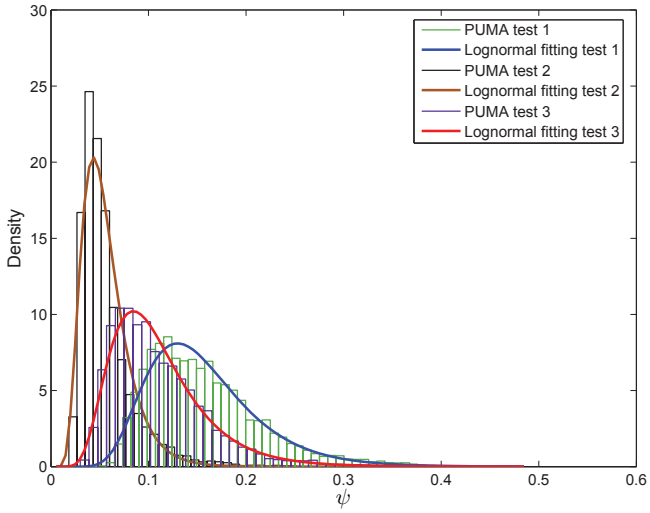

Figure 3. Histogram distributions and fitted log-normal PDFs for the experiments with the Puma 260 robot.

results of these experiments have shown that the log-normal is a good choice for characterizing the detection index $\psi(t)$. This result will be used in the following section to define a procedure for the automatic tuning of the threshold ε.

4.3 Procedure for tuning the detection threshold

According to the experimental results of Section 4.2 and to the characterization of the distribution of $\psi(t)$ as a log-normal, we can define a procedure for tuning the detection threshold ε as follows:

1. Given initial values of inertia and damping matrices and, therefore, of the desired damping to inertia ratio matrix, the experienced operator applies persistent force stimuli to the admittance-controlled robot to move it in a wide portion of its workspace, while the control system logs the values of $\psi(t)$ for at least 60 seconds.

2. The potential presence of a significant number of outliers in the recorded series of $\psi(t)$ is detected. Indeed, outlying samples are potentially related to undesired oscillations that even the experienced user may have not perceived. Being the log-normal a *skewed* distribution, the outliers detection is based on the adjusted boxplot described in Hubert and Vandervieren (2008). Following this approach, a sample is considered to be an outlier if it falls outside of the interval:

$$\left[Q_1 - 1.5e^{-4MC}\mathrm{IQR},\ Q_3 + 1.5e^{3MC}\mathrm{IQR}\right] \qquad (10)$$

where Q_1 and Q_3 are respectively the first and third quartile of the sampled data, $\mathrm{IQR} = Q_3 - Q_1$ is the interquartile range and MC is the *medcouple*, a robust measure of skewness (Brys et al. (2004)). Note that the proposed boxplot formula assumes $MC > 0$, since a log-normal distribution is *right* skewed. If the total number of outliers does not exceed 5% of the sampled data and consecutive outlying samples represent short time intervals (e.g. smaller than 200 ms), it can be concluded that experimental data do not include oscillating behaviors and can be used for the subsequent steps of the tuning procedure.

3. If outliers are negligible and the user acknowledges that the experimental run is valid for the tuning of the threshold, the PDF of $\psi(t)$ is estimated from sampled data. In particular, the parameters of a log-normal distribution are estimated using the following MLE formulas (see Ginos (2009)):

$$\hat{\mu} = \frac{\sum_{i=0}^{N-1} \ln \psi(i \cdot T)}{N}; \quad \hat{\sigma} = \sqrt{\frac{\sum_{i=0}^{N-1} \left(\ln \psi(i \cdot T) - \hat{\mu}\right)^2}{N}} \qquad (11)$$

where T is the sampling period, N is the number of discrete-time samples of $\psi(t)$ collected during the test, $\hat{\mu}$ and $\hat{\sigma}$ are the estimated *location* and the estimated *scale* of the log-normal distribution (Johnson et al. (1995)), respectively.

4. The threshold ε is fixed as the upper bound of the prediction interval calculated as the value at which the log-normal CDF reaches the confidence level $\alpha = 0.9999$ (chosen with the aim to mostly avoid false positive detections).

In order to validate the proposed method, we applied the described procedure on the data of the experiments reported in Figures 2 and 3. Table 1 shows the threshold ε that resulted from tests 1, 2 and 3 being performed on each robotic setup by a specific user. Obviously, the value of the threshold changes depending on the damping to inertia ratio and on the robot being used. However, repeating each test with different (experienced) users and with different admittance parameters values (keeping a constant damping to inertia ratio) led to threshold values (not fully reported here for conciseness) changing only within a ± 5 % interval with respect to those reported in Table 1. Therefore, we can conclude that, under Assumption 4, the threshold, automatically computed from a test run by an experienced user, can be used for online detection of rising oscillations.

Table 1. Resulting detection threshold ε in different tests.

	test 1	*test 2*	*test 3*
KUKA LWR 4+	1.015	0.1698	0.4379
PUMA 260	0.5544	0.2410	0.4871

5 Methodology for parameter adaptation with weighted energy allocation

5.1 Passivity-based approach for restoring the desired behavior

In this section we will show how to adapt the parameters of the admittance control to restore the desired behavior of the controlled robot in the presence of high-frequency oscillations, identified according to the technique described in Section 4. If the parameters have to be adapted, then the desired interaction model becomes the variable admittance model (4). The main drawback due to the introduction of

variable terms in an admittance control scheme is the loss of passivity of the controlled robot (see, e.g., Ferraguti et al. (2015)). This can be easily seen by considering the non negative total energy as a storage function:

$$H(\dot{x}(t)) = \frac{1}{2}\dot{x}(t)^T M(t)\dot{x}(t) \tag{12}$$

The variation of the energy function is given by:

$$\dot{H}(\dot{x}(t)) = \dot{x}(t)^T M(t)\ddot{x}(t) + \frac{1}{2}\dot{x}(t)^T \dot{M}(t)\dot{x}(t) \tag{13}$$

Using (4) in (13) we obtain:

$$\dot{H}(\dot{x}(t)) = \dot{x}(t)^T F(t) + \frac{1}{2}\dot{x}(t)^T \left(\dot{M}(t) - 2D(t)\right)\dot{x}(t) \tag{14}$$

Due to the variability of the inertia matrix, the term between brackets can be positive and, therefore, some extra energy can be injected into the system by the controller. This effect would destroy passivity and lead to a potentially unstable and unsafe behavior of the robot.

In order to guarantee the passivity, we exploit the concept of energy tanks that allows to use the (virtual) energy circulating in the controlled system in a flexible and passivity preserving way (see, e.g., Secchi et al. (2006); Franken et al. (2011); Ferraguti et al. (2015)). Indeed, the energy dissipated by the system is stored in a virtual energy reservoir, the *tank*, and can be reused for implementing any desired control action in a passivity preserving way. For this purpose, we augment the dynamics (4) as follows:

$$\begin{cases} M(t)\ddot{x}(t) + D(t)\dot{x}(t) = F(t) \\ \dot{z}(t) = \dfrac{\varphi(t)}{z(t)}P_D(t) - \dfrac{\gamma(t)}{z(t)}P_M(t) \end{cases} \tag{15}$$

where

$$P_D(t) = \dot{x}(t)^T D(t)\dot{x}(t) \qquad P_M(t) = \tfrac{1}{2}\dot{x}(t)^T \dot{M}(t)\dot{x}(t) \tag{16}$$

are the dissipated power due to the damping, and the dissipated/injected power due to the inertia variation, respectively, and $z(t) \in \mathbb{R}$ is the state of the tank. Furthermore, let

$$T(z(t)) = \frac{1}{2}z(t)^2 \tag{17}$$

be the energy stored in the tank. We will hereafter assume that $\exists \delta, \bar{T}$, with $0 < \delta < \bar{T}$, such that $\delta \leq T(z(t)) \leq \bar{T}$, $\forall t$. The upper bound is guaranteed by the parameters $\varphi(t) \in \{0,1\}$ and $\gamma(t) \in \{0,1\}$ that disable the energy storage in case a maximum, application dependent, limit $\bar{T} \in \mathbb{R}^+$ is reached. It is necessary to bound the available energy because, if there were no bounds, the energy could become very big as time increases and, even if the system keeps on being passive, it would be possible to implement practically unstable behaviors (Lee and Huang (2010)). In particular,

$$\varphi(t) = \begin{cases} 1 & \text{if } T(z(t)) \leq \bar{T} \\ 0 & \text{otherwise} \end{cases} \tag{18}$$

enables/disables the storage of dissipated energy, while

$$\gamma(t) = \begin{cases} \varphi & \text{if } \dot{M}(t) \leq 0 \\ 1 & \text{otherwise} \end{cases} \tag{19}$$

enables/disables the injection $\left(\dot{M}(t) \leq 0\right)$ of energy in the tank due to the inertia variation but it always allows to extract $\left(\dot{M}(t) > 0\right)$ energy from the tank. The lower bound, required for avoiding singularities in (15), is guaranteed by carefully planning/forbidding the extraction of energy when $T(z(t)) = \delta$ is reached. Notice that the extraction of energy is due only to $P_M(t)$. The tank initial state is set to $z(0)$ such that $T(z(0)) > \delta$.

The evolution of the energy in the tank can be written as:

$$\dot{T}(z(t)) = z(t)\dot{z}(t) = \varphi(t)P_D(t) - \gamma(t)P_M(t) \tag{20}$$

Using the augmented dynamics it is possible to prove the following result:

Proposition 1. *If $T(z(t)) \geq \delta$ for all $t \geq 0$, the system (15) is passive with respect to the pair $\left(F(t), \dot{\tilde{x}}(t)\right)$.*

Proof. Consider the following positive storage function:

$$W\left(\dot{x}(t), z(t)\right) = H\left(\dot{x}(t)\right) + T(z(t)) \tag{21}$$

where $H(\dot{x}(t))$ is defined in (12) and $T(z(t))$ in (17). With a slight abuse of notation we will hereafter use $W(t)$, $H(t)$ and $T(t)$ to indicate, respectively, the value of $W\left(\dot{x}(t), z(t)\right)$, $H\left(\dot{x}(t)\right)$ and $T(z(t))$ at time t. We have that:

$$\begin{aligned} &\dot{W}(t) = \dot{H}(t) + \dot{T}(t) = \\ &\dot{x}(t)^T F(t) - \left(1 - \varphi(t)\right) P_D(t) + \left(1 - \gamma(t)\right) P_M(t) \end{aligned} \tag{22}$$

Since $\varphi(t) \in \{0,1\}$ and $P_D(t) \geq 0$, we have that

$$\dot{x}(t)^T F(t) \geq \dot{H}(t) + \dot{T}(t) - \left(1 - \gamma(t)\right) P_M(t) \tag{23}$$

If $\dot{M}(t) \leq 0$, then, from (16) and from (19). it follows that $-\left(1 - \gamma(t)\right) P_M(t) \leq 0$. In case $\dot{M}(t) > 0$, from (19), it follows that $\gamma(t) = 1$ and, consequently, $\left(1 - \gamma(t)\right) P_M(t) = 0$. Thus, from (22) we can obtain:

$$\dot{x}(t)^T F(t) \geq \dot{H}(t) + \dot{T}(t) \tag{24}$$

which implies

$$\int_0^t \dot{x}(\tau)^T F(\tau)\, d\tau \geq H(t) - H(0) + T(t) - T(0) \geq -H(0) - T(0) \tag{25}$$

which proves passivity. □

Thus, as long as there is energy available in the tank, it is possible to implement any kind of inertia variation. Nevertheless, it is important to guarantee that the variation of the inertia does not deplete the tank. Indeed, if this happens, all the active behaviors (e.g. increasing of inertia) would be stopped and this would lead to unwanted behaviors (e.g. oscillations) in the cooperative system. In the following we propose a condition on the variation of the inertia that guarantees that the tank never depletes and, as a consequence, that the system remains passive.

We assume that the inertia variations take place in predefined finite intervals (e.g. when the user stiffens his/her arm). As clearly shown in (15) and in (16), energy can be extracted by the tank only if $\dot{M}(t) > 0$. Thus, it is necessary to bound the increase of inertia depending on the energy stored in the tank. Consider a generic time interval $[a, b]$

where $\dot{M}(t) > 0$. From (19), $\gamma(t) = 1$ for all $t \in [a, b]$. From (20), the energy of the tank at $t = b$ is given by:

$$T(b) = T(a) + \int_a^b P_D(\tau)d\tau - \int_a^b P_M(\tau)d\tau \geq T(a) - \int_a^b P_M(\tau)d\tau \tag{26}$$

In order to avoid to deplete the tank during the variation interval, since $\dot{M}(t) > 0$ for all $t \in [a, b]$, it is sufficient that $T(b) \geq \delta$, namely, using (26):

$$T(a) - \int_a^b P_M(\tau)d\tau \geq \delta \tag{27}$$

which can be reformulated as:

$$\int_a^b P_M(\tau)d\tau \leq T(a) - \delta \tag{28}$$

namely that the energy extracted in the interval is at most equal to the energy initially available beyond the lower bound δ.

Since the desired inertia and damping are parameters that can be freely chosen, provided that they are symmetric and positive definite matrices, we will consider the following assumption.

Assumption 5. *The desired inertia and damping in (4) are diagonal matrices and they are defined as*

$$\begin{aligned} M(t) &= \text{diag}\,\{m_1(t), \ldots, m_6(t)\} \\ D(t) &= \text{diag}\,\{d_1(t), \ldots, d_6(t)\} \end{aligned} \tag{29}$$

Since $M(t)$ is diagonal, $\dot{M}(t)$ is diagonal too and its eigenvalues are the elements on the diagonal.

With this assumption, we can decouple the different components (e.g. the translational components from the rotational ones). Indeed, the following inequality holds:

$$\int_a^b P_M(\tau)d\tau \leq \sum_{j=1}^{6} \frac{1}{2}\bar{m}_j \bar{\dot{\mathcal{X}}}_j^2 (b - a) \tag{30}$$

where $\bar{m}_j$ $(j = 1, \ldots, 6)$ are bounds on $\dot{m}_j(t)$ for all $t \in [a, b]$ and $\bar{\dot{\mathcal{X}}}_j = \max_q \dot{\mathcal{X}}_j(q)$ $(j = 1, \ldots, 6)$ are component-wise upper bounds on the robot velocity limits defined in Assumption 1. On the other hand, if we define a vector of weights $\mathcal{A} = \{\alpha_1, \ldots, \alpha_6\}$, such that:

$$\sum_{j=1}^{6} \alpha_j = 1 \tag{31}$$

and we use these weights to distribute the energy available in the tank at the beginning of the adaptation period on the 6 DOFs of robot motion:

$$T(a) - \delta = \sum_{j=1}^{6} \alpha_j (T(a) - \delta) \tag{32}$$

then it is possible to write the following inequalities:

$$\frac{1}{2}\bar{m}_j \bar{\dot{\mathcal{X}}}_j^2 (b - a) \leq \alpha_j (T(a) - \delta) \quad \forall j = 1, \ldots, 6 \tag{33}$$

Consequently, the condition on the inertia variations that allows to preserve passivity, with a weighted distribution of the energy extracted from the tank within the adaptation interval, can be stated as follows:

$$\dot{m}_j(t) \leq \bar{m}_j \leq \frac{2\alpha_j (T(a) - \delta)}{\bar{\dot{\mathcal{X}}}_j^2 (b - a)} \quad \forall j = 1, \ldots, 6 \tag{34}$$

This newer formulation of the passivity-preserving adaptation law, with respect to the one used in Talignani Landi et al. (2017a,b), allows to take into account that the velocity bounds of the robot may be quite different on the different DOFs, especially comparing translational and rotational ones. Thanks to the component-wise definition of the inertia variation bound and to a proper choice of the weights vector $\mathcal{A}$, the adaptation of the admittance parameters related to each DOF can be tuned more precisely, according to the features of the robot and to the desired task. Intuitively, lower weights should be specified for the components related to rotational DOFs, whose corresponding elements on the diagonal of $M(t)$ tends to be smaller than those related to translational DOFs (i.e. the values in the inertia tensor of a rigid body are, in general, quantitatively smaller than its mass). On the other hand, the oscillating behavior of the human-robot interaction can be counteracted with smaller inertia variations on those DOFs for which higher velocities are admissible. More details on the tuning of the weights vector will be given in Section 6.

5.2 Algorithm for parameter adaptation in admittance control

Section 5.1 provided a possible way for using (34) to adapt the parameters of the admittance control to recover a stable behavior of the human-robot interaction when oscillations are detected. In the following we will provide a procedure for parameter adaptation, that allows to increase the parameters only when it is required due to the detection of rising oscillations, but then restores the desired interaction model when such oscillations disappear (e.g. due to a relaxation of the operator's arm). The parameters will be adapted according to the component-wise passivity-preserving bound defined by (34). The algorithm will be provided in the discrete-time domain in order to be implementable on a real robotic system. The conditions on the time derivatives stated so far can be approximated using the corresponding difference quotient for a sufficiently small sampling period. We will then consider a set of time intervals $[t_i, t_{i+1}]$, with $i = 1, 2, \ldots$ and such that $t_{i+1} - t_i = \Delta t$, within which the parameter adaptation takes place. In particular, Algorithm 1 shows how the admittance parameters are updated.

Once rising oscillations have been detected, the algorithm allows to compute the variation of the inertia that satisfies the passivity constraints and the stability of the system is recovered. The variation of the damping is performed according to a constant damping to inertia ratio ($R_d(t) = R_d(0), \forall t \geq 0$). Thus, the first step of the algorithm is the computation of the damping to inertia ratio according to (8) and based on the desired inertia matrix $M(0)$ and damping matrix $D(0)$ (Line 2). Then, at each time instant t_i, the detection index defined in (9) is computed (Line 4). If oscillations are rising, (9) is not satisfied and the oscillatory behavior is detected in Line 5, where $\varepsilon > 0$ is a threshold previously defined using the procedure proposed

Algorithm 1: Parameter Adaptation

Data: $M(0), D(0), \beta, \varepsilon, \Delta t, \Delta M, \mathcal{A}$
1 initialize $k = 0, \zeta_0 = 0, \zeta = \{\zeta_0\}, S_0 = 0_6$
2 compute damping to inertia ratio: $R_d(0) = M^{-1}(0)D(0)$
3 **for** $i = 0$ **to** ∞ **do**
4 compute the detection index $\psi(t_i) = \|\ddot{\tilde{x}}(t_i) + R_d(0)\dot{\tilde{x}}(t_i)\|$
5 **if** $\psi(t_i) > \varepsilon$ **then**
6 $k = k + 1$
7 update vector of oscillations occurrences $\zeta_k = t_i$
8 **for** $j = 1$ **to** 6 **do**
9 compute amount of inertia variation
$$s_j = \min\left\{\frac{2\alpha_j\left(T(t_i) - \delta\right)}{\dot{\bar{\mathcal{X}}}_j^2}, \bar{m}_j\right\}$$
10 **end**
11 $S_i = \mathrm{diag}\left\{s_1, \ldots, s_6\right\}$
12 **end**
13 update inertia
$$M(t_{i+1}) = M(0) + \sum_{p=0}^{k} S_p \beta^{\left(t_{i+1} - (\zeta_p + \Delta t)\right)}$$
14 update damping $D(t_{i+1}) = R_d(0)M(t_{i+1})$
15 **end**

in Section 4. The vector ζ stores all the instants in which oscillations are detected. Thus, at Line 7 a new element ζ_k is inserted in ζ and it is associated to the current instant of time t_i which corresponds to the instant of detection. In this case, the admittance parameters have to be adapted for restoring the stability of the system. In particular, under condition (33) and Assumption 5, integrating (34), we obtain that each component of the inertia matrix can be passively increased as follows

$$m_j(t_{i+1}) - m_j(t_i) = \frac{2\alpha_j(T(t_i) - \delta)}{\dot{\bar{\mathcal{X}}}_j^2} \quad \forall j = 1, \ldots, 6 \tag{35}$$

It is worth noting that (35) represents the maximum allowed inertia variation, based on the energy contained in the tank at time $t = t_i$. In practical cases, this value can be very large: thus, direct application of (35) would lead to an excessively large inertia variation. For this reason, we define an upper-bound $\Delta M = \mathrm{diag}\{\bar{m}_1, \cdots, \bar{m}_6\}$ on the allowed inertia variation as follows:

$$m_j(t_{i+1}) - m_j(t_i) \leq \bar{m}_j \quad \forall j = 1, \ldots, 6 \tag{36}$$

Under such a condition, the amount of variation of the inertia can be computed component-wise as the minimum between the allowed inertia variation (35) and the upper-bound (36) (Line 9):

$$s_j = \min\left\{\frac{2\alpha_j(T(t_i) - \delta)}{\dot{\bar{\mathcal{X}}}_j^2}, \bar{m}_j\right\} \quad \forall j = 1, \ldots, 6 \tag{37}$$

The empirical definition of the bounds $\bar{m}_j$ is a practical necessity and has been exploited in the experiments described in Talignani Landi et al. (2017a,b) also to take into account that some DOFs (i.e. generally rotational ones) may require smaller values of inertia variations. However, the newer definition of the inertia adaptation law, based on the weighted distribution of the tank energy, allows to modulate more precisely the inertia variations, thanks to the choice of the weights vector and the component-wise scaling by the velocity bounds $\dot{\bar{\mathcal{X}}}_j$. Indeed, in the experiments reported in Section 6, the conservative bounds $\bar{m}_j$ were rarely enforced.

The single components computed in (37) are then used in Line 11 to fill the matrix of inertia variation as follows:

$$S_i = \mathrm{diag}\left\{s_1, \ldots, s_6\right\} \quad \forall i = 1, 2, \ldots \tag{38}$$

The final part of the algorithm is the actual variation of the admittance parameters. The inertia variation is computed in Line 13 as follows:

$$M(t_{i+1}) = M(0) + \sum_{p=0}^{k} S_p \beta^{\left(t_{i+1} - (\tau_p + \Delta t)\right)} \tag{39}$$

where β $(0 < \beta \leq 1)$ is a forgetting factor that allows to gradually restore the desired interaction model (3). Indeed, the presence of the forgetting factor β in the second term in the right-hand side of (39) makes the effect of each inertia increase negligible after a certain amount of time. In particular, this time is larger for higher values of β. Note that the inertia increases only at each time instant when a deviation is detected, as a consequence of (39). In all the other instants, the inertia only decreases and this has been shown in Talignani Landi et al. (2017b) to be a passivity-preserving operation.

Finally, the damping is updated preserving the constant damping to inertia ratio as follows:

$$D(t_{i+1}) = R_d(0)M(t_{i+1}) \tag{40}$$

6 Experiments

The proposed adaptation strategy has been validated by means of experiments performed on two different robotic systems and involving a total of 50 users (13 female, 37 male, from 22 to 44 years old), divided into four groups: two of 12, one of 15 and one of 18 users. Since industrial tasks typically require a combination of precision and execution speed, we implemented two tasks focused on the two separate aspects. Each group of users was asked to interact with one of the robots to perform one of the tasks. Therefore, the four groups experienced two different tasks on two different robots, with a minimal overlap of people in the four experiences. The two robotic setups consisted of:

- a Puma 260 6-DOF robot with a retrofitted control hardware, embedding six Gold Solo Whistle servo drives from Elmo Motion Control, and a wrist-mounted 6-axis F/T sensor, made by the IIT research institute;
- a KUKA LWR 4+ 7-DOF robot, equipped with a ATI Mini 45 6-axis F/T sensor and configured in its (non-compliant) joint position control mode.

The control software has been implemented using the Orocos Real-Time Toolkit (RTT) and Kinematics/Dynamics Library (KDL)[†] and is the same on the two robots, excluding only hardware interface components (i.e. using the Fast Research Interface on the KUKA robot and the EtherCAT

[†]http://www.orocos.org

fieldbus on the Puma 260). Even the sampling times of the admittance controller and of the parameter adaptation algorithm, respectively set to 2 ms and 4.5 ms, are the same on the two systems.

Velocity and acceleration limits of the two robots are imposed, at joint level, by the servo drives on the Puma 260 and by a bank of nonlinear filters (Gerelli and Bianco (2009)) smoothing the joint position commands on the KUKA LWR 4+. In this way, such limits can be arbitrarily configured on both systems, while the joint position control mode of the KUKA LWR 4+ would not provide this feature. Cartesian velocity and acceleration limits (i.e. $\dot{\mathcal{X}}(q)$ and $\ddot{\mathcal{X}}(q)$) are then computed online via the Jacobian and Jacobian derivative matrices depending on the current joints configuration. In this way the detection index $\psi(t)$ is precisely computed according to (9) on the basis of the dynamic bounds corresponding to the current robot pose. A constant upper bound for the velocity limits (i.e. $\bar{\dot{\mathcal{X}}}$) to be used for the admittance control adaptation law (35), was then defined after experimental observations performed in the reduced part of the workspace interested by the two tasks. In particular, the velocity bounds to be used in (35) are fixed as $\bar{\dot{\mathcal{X}}} = \{2.50, 2.50, 2.50, 24, 24, 24\}$ for the Puma 260 and $\bar{\dot{\mathcal{X}}} = \{2.30, 2.30, 2.30, 6, 6, 6\}$ for the KUKA LWR 4+. The vectors of weights, whose components are used in (35) to distribute the energy available in the tank during the adaptation, are set to $\mathcal{A} = \{0.25, 0.25, 0.25, 0.1, 0.1, 0.05\}$ for the Puma 260 and $\mathcal{A} = \{0.3, 0.3, 0.3, 0.04, 0.04, 0.02\}$ for the KUKA LWR 4+. This choice of the velocity bounds and of the weights vectors in (35) allows to achieve similar adaptive behaviors on the two robots.

According to the theory developed in Sections 3 and 5, some design choices were made. In particular, the energy thresholds, required by the passivity-preserving mechanism of Section 5, have been selected as $\delta = 0.1\ J$ and $\bar{T} = 5\ J$. The initial value for the state of the tank is set to $z(0) = 2$, so that the initial energy contained in the tank, computed according to (17) results in $T(0) = 2\ J > \delta$.

The objective of the proposed experiments is to validate usability and portability across different robotic systems of the proposed adaptive admittance control method, even in absence of an accurate and, possibly, task-dependent or robot-dependent tuning of the admittance parameters. For this reason, we used the same initial values of admittance control parameters on both robots and for both interaction tasks. In particular, such values of the inertia and damping matrices were set as:

$$M(0) = \text{diag}\{M_1, M_2\} \quad D(0) = \text{diag}\{D_1, D_2\} \qquad (41)$$

with

$$M_1 = \text{diag}\{1, 1, 1\}\ kg \quad M_2 = \text{diag}\{0.1, 0.1, 0.1\}\ {}^{kg}/_{m^2}$$

$$D_1 = \text{diag}\{4, 4, 4\}\ {}^{Ns}/_{m} \quad D_2 = \text{diag}\{0.4, 0.4, 0.4\}\ {}^{Nms}/_{rad}$$

Finally, same values were used on both robots for the time interval of the adaptation, set to $\Delta t = 4.5\ ms$, the forgetting factor, chosen as $\beta = 0.98$, and the upper bounds on inertia variation, i.e. $\Delta M = \text{diag}\{0.5, 0.5, 0.5, 0.005, 0.005, 0.005\}$.

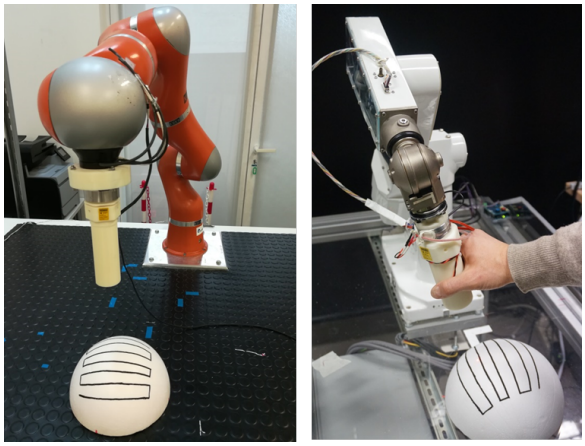

Figure 4. Setup of the laser tracking task on the Kuka LWR 4+ (left) and on the Puma 260 (right).

In the following we will present the two tasks that emulate industrial applications involving manual guidance of the manipulators, and the results collected during the interaction of the 50 users with the robots. Moreover, the users were asked to fill the questionnaire proposed in Schmidtler et al. (2017) in order to obtain a qualitative evaluation of the human-robot interaction from the user's perspective. The two tasks have been implemented on both robotic setups.

6.1 *Precision task: tracking a line on a spherical surface*

In the first task, the users were asked to manually drive the end-effector of the robot, equipped with a handle embedding a laser pointer. The goal was to track, with the light dot, a path drawn on the surface of a sphere. This kind of task emulates industrial applications where the robotic tool has to precisely follow a contour (e.g. welding). All the DOFs of the manipulator are involved. Figure 4 shows the setup of the two robotic systems for the laser tracking task.

More precisely, the task involves the following steps:

- The user grabs the handle, which is initially far from the spherical target, and brings it as fast as possible towards the drawn path.
- When the handle is at 10 cm from the sphere, the laser pointer is switched on automatically and a timer measuring the task completion time is started.
- The user has to lead the light dot through the drawn path, from a given initial point to a given ending point and back, as quickly as possible and keeping the light dot as close as possible to the path.

The data collected during the experiment are used to extract a quantitative evaluation of the task execution, in terms of: task completion time; number of zero-crossings in the Cartesian velocities of the robot end-effector (i.e. quantifying the smoothness of the task execution); root mean square (RMS) of the tracking error, measured as the distance from the projection of the light dot on the sphere to the closest point on the path; RMS of the force/torque vector measured by the F/T sensor on the handle.

A group of 12 users interacted with the KUKA LWR 4+ and a group of 18 users interacted with the Puma 260. In both cases, each user performed the task three times, with a different setting of the adaptation strategy, namely:

- **Control Mode 1:** The adaptation mechanism is triggered according to the detection threshold properly tuned with the procedure defined in Section 4, that resulted as $\varepsilon = 0.16$ on the Puma robot and $\varepsilon = 0.2$ on the KUKA robot. The damping to inertia ratio is computed from the parameters (41).
- **Control Mode 2:** The adaptation mechanism is triggered according to a detection threshold either under-estimated (on the KUKA setup, i.e. modifying $\varepsilon = 0.1$) or over-estimated (on the Puma setup, i.e. modifying $\varepsilon = 0.32$), to evaluate the effects of, respectively, an unnecessarily frequent or an untimely adaptation. The damping to inertia ratio is the same as the previous control mode.
- **Control Mode 3:** The adaptation mechanism is disabled and the admittance controller has the following constant parameters, much higher than the initial values of the adaptive model:

$$M_d = \text{diag}\{M_{d1}, M_{d2}\} \quad D_d = \text{diag}\{D_{d1}, D_{d2}\}$$

with

$$M_{d1} = \text{diag}\{8, 8, 8\}\ kg \quad M_{d2} = \text{diag}\{0.25, 0.25, 0.25\}\ {}^{kg}/_{m^2}$$

$$D_{d1} = \text{diag}\{32, 32, 32\}\ {}^{Ns}/_{m} \quad D_{d2} = \text{diag}\{1.0, 1.0, 1.0\}\ {}^{Nms}/_{rad}$$

Since users were not allowed to test the system before the three experiments, the control modes were applied in a random order for each user, to avoid that numerical results could be affected more by the self-training induced by previous execution of the task, rather than by the control mode itself.

The first result that we could observe is related to the influence of the detection threshold on the adaptive admittance control behavior. Indeed, experiments on the KUKA robot with an under-estimated threshold revealed a mean number of adaptations per user of 16.75 (maximum 31, user #9), while in the experiments with the properly tuned threshold the mean was 5.33 (maximum 15, user #10). Conversely, the mean number of adaptations on the Puma robot with an over-estimated threshold was 1.22 (maximum 9, user #18), smaller than the mean of 2.94 (maximum 11, user #4) of the experiments with the properly tuned threshold. It should also be remarked that the number of adaptations is not as large as could be expected, considering that the initial values of the admittance parameters are set purposefully low and, therefore, prone to generating oscillations. However, the laser tracking task induced the users to focus more on the tracking performance, rather than focusing on the completion time, and this behavior led them to apply soft and smooth inputs to the handle. As a consequence, the maximum values on the inertia matrix did not change much with respect to the initial setting. Figure 5 shows the maximum inertia values reached during the task being performed on the KUKA robot. Similar results were obtained on the Puma setup.

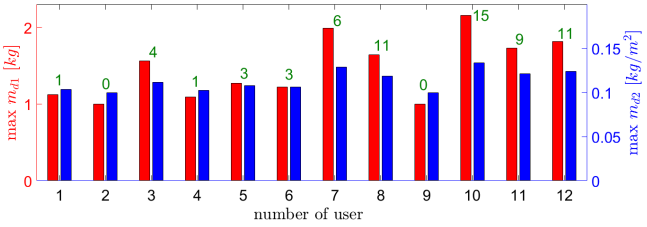

Figure 5. Laser tracking task on KUKA LWR 4+: maximum values of the inertia reached through the parameter adaptation, on translational DOFs (red columns) and rotational DOFs (blue columns). The number of detections triggering the adaptation is reported on top of the columns.

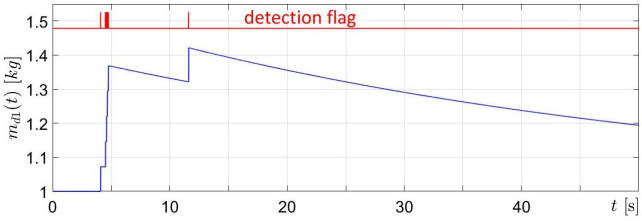

Figure 6. Evolution over time of the inertia on a translational DOF for one user performing the laser tracking task, with properly tuned detection threshold, on the Puma 260 setup.

Another interesting aspect of the adaptation results is the fact that the inertia increasing mechanism was most frequently triggered at the beginning of the experiment, when the user had to grab the handle and to bring the robot near to the sphere. Indeed, during this phase users were more focused on the rapidity of motion and, therefore, they grabbed the handle more firmly and applied sharper forces. As an example, Figure 6 shows the evolution over time of the inertia along the x-direction for the experiment being performed by user #7 on the Puma 260.

The quantitative results collected during the task execution have been evaluated applying a two-way analysis of variances (ANOVA), with the aim to compare the effect of control mode and user-specific capabilities as the two factors influencing the observations. Table 2 shows the p-values that resulted for the laser tracking task. A p-value lower than a given significance level (generally 0.05) suggests that there is a relevant effect due to the related factor. The results show that the only quantity that is significantly influenced by the control mode is the RMS value of the force input, while most of the other quantities are only influenced by the capabilities of the user. In other words, there were faster and slower users, but both fast and slow users obtained very similar performances with each control mode. Instead, no significant differences on the tracking errors are found. On the other hand, the number of velocity zero-crossings is not significantly influenced by the control mode, revealing that the adaptation mechanism allows to promptly inhibit rising oscillations, so that human-robot interactions are as smooth as those governed by fixed high values of admittance control inertia and damping. The high values of the parameters imposed in control mode 3, however, play an important role on the physical effort required to the human, measured by the force RMS. The increased effort is clearly evident in Figure 7, where the three control modes are compared in terms of RMS of the force applied by the user during the

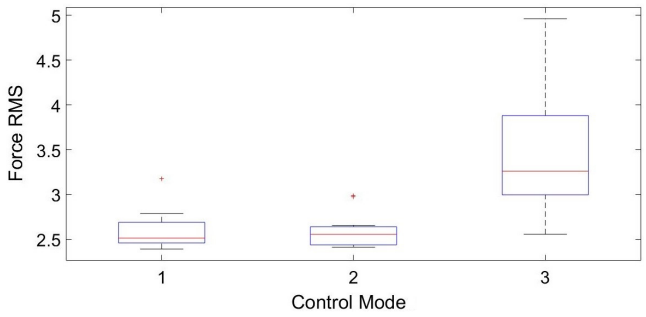

Figure 7. Boxplots that compare the RMS of the force applied by the user to drive the robot during the laser tracking task on the KUKA setup and with the three control modes.

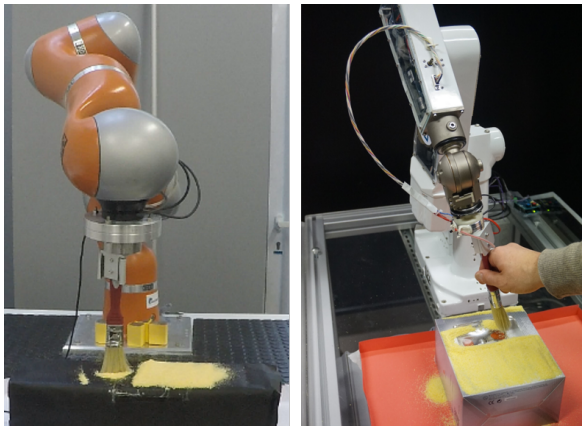

Figure 8. Setup of the brushing task on the Kuka LWR 4+ (left) and on the Puma 260 (right).

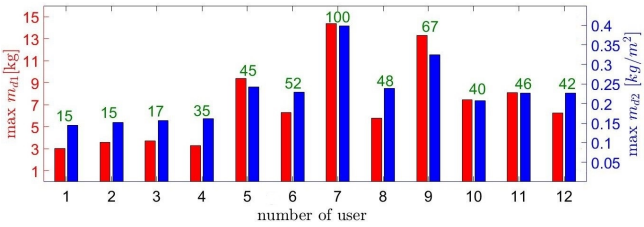

Figure 9. Brushing task on KUKA LWR 4+: maximum values of the inertia reached through the parameter adaptation, on translational DOFs (red columns) and rotational DOFs (blue columns). The number of detections triggering the adaptation is reported on top of the columns.

task execution. Indeed, control modes 1 and 2 required a reduced effort to the user, since the adaptation algorithm allows to set low initial inertia and damping parameters that are automatically adapted if oscillations arise.

Finally, a subjective qualitative evaluation has been obtained asking users to fill the questionnaire for Physical Assistive Devices (QUEAD) proposed in Schmidtler et al. (2017), including a total of sixteen statements, to be scored with a number from 1 (entirely disagree) to 7 (entirely agree), and related to five aspects of human-robot interaction: usefulness, ease of use, emotions, attitude and comfort. Users were instructed to refer their evaluation to the adaptive control mode with the properly tuned detection threshold (control mode 1), but also to give their order of preference for the three control modes tested. Table 3 shows that the mean values of the qualitative evaluation are high (always higher than 4.75 out of maximum level of 7) on all the features. Moreover, the order of preference was evaluated by giving 3 points to the preferred control mode, 2 points to the second best and 1 point to the last preferred. Summing the results of the 30 users testing either the Puma or the KUKA, the adaptive control mode with properly tuned threshold obtained 66 points, the non-adaptive control mode 63 and the adaptive control mode with under-estimated or over-estimated threshold 51. It is important to remark that these results are actually influenced by the choice of the initial parameters of inertia and damping. Indeed, high admittance parameters have been chosen when the users tested the non-adaptive control mode, in order to avoid frequent instabilities and oscillations. If lower parameters were chosen, users could have better appreciate the advantages of the adaptive control mode, but it may have been more difficult for them to complete the task, due to frequent instabilities. Moreover, it can be noted that the adaptive control mode with under-estimated or over-estimated threshold is rated lower than the non-adaptive control mode. This result is not surprising, since the detection threshold is a critical parameter in the proposed method. If the threshold is not tuned correctly, the results of the adaptation can be even worse with respect to the standard admittance control with high parameters. From this, one can assess the importance of an automatic tuning procedure of the detection threshold, as the one proposed in Section 4.3, eliminating the chance for wrong threshold estimation.

6.2 *Rapidity task: brushing off a flat surface*

In the second task, a soft brush has been mounted on the end-effector of the robots, as shown in Figure 8, and users were asked to clean a flat surface from a colored dust, applying motions mimicking a painting task. In this case, precise movements are not required and the task completion time becomes the most significant quantitative aspect. Since the role of the detection threshold has been already shown by the results of the laser tracking task, the brushing task has been executed by the users only with the properly tuned adaptive control mode (control mode 1) and with the non-adaptive one (control mode 3).

Users were instructed to execute the operation as fast as possible. This objective induced the users to grab strongly the brush and apply high and sharp forces, leading to high levels of rising oscillations in the human-robot interactive behavior. As a result, the parameter adaptation strategy was triggered much more frequently compared to the laser tracking task. Figure 9 shows the inertia values of the 12 users that performed the task with the KUKA robot. Similar results were obtained on the Puma setup.

The results of the two-way ANOVA, reported in Table 4, are related to the same quantities recorded for the laser tracking task, excluding the tracking error RMS. The table shows that the control mode has a strong influence on the number of zero-crossings for the experiments performed on the Puma robot, but not for the experiments performed on the KUKA setup. In our opinion, this result is motivated by the fact that the Puma robot has a smaller workspace than the KUKA's one and thus the users had to work

Table 2. Results of two-way ANOVA on user tests for the laser tracking task.
p-values lower than 0.05 (yellow cells) suggests that there is a relevant effect due to the related factor.

Setup		Time		Zero Crossings		Force RMS		Tracking Error RMS	
		mode	users	mode	users	mode	users	mode	users
PUMA	p-value	0.499	**0**	0.511	**0**	**0.006**	**0**	0.511	0.609
KUKA	p-value	0.203	**0**	0.345	**<0.001**	**0**	0.097	0.297	0.2565

Table 3. Results of qualitative evaluations of the laser tracking task with QUEAD (Schmidtler et al. (2017)).

Setup	Usefulness	Ease of use	Emotions	Attitude	Comfort
PUMA	4.75	5.15	5.03	5.05	4.94
KUKA	5.33	5.6	5.51	5.5	6.11

on a smaller surface and were induced to perform shorter motion cycles, repeated several times. This behavior resulted in purposefully oscillating behaviors in control mode 1 (small initial inertia and damping) that produced a higher number of velocity zero-crossings, even though not all of these oscillations triggered the parameter adaptation. On the KUKA setup, instead, users had to clean a bigger surface and they generally applied motions cycles with a larger range, but repeated less frequently. This behavior can also be related to a stronger grasp on the brush and a higher RMS value of the applied force, both with the adaptive control mode and with the non-adaptive one. Indeed, the ANOVA result about the effect of control mode on force RMS is not significant.

The results of the qualitative evaluation with the QUEAD, reported in Table 5, are slightly higher than those collected for the tracking task. Moreover, when asked to indicated their preferred control mode, 21 of the 27 total users selected the adaptive admittance control, which is a more definite preference compared with the one expressed on the laser tracking task.

6.3 *Adaptation strategy assessment and comparison*

In order to demonstrate the effectiveness of the overall detection and adaptation strategy, we performed experiments to show how the heuristic introduced in Section 4 detects the oscillatory behavior of the robots and the way stability is restored thanks to the adaptation strategy presented in Section 5. Moreover, experiments to compare the proposed approach with state-of-the art methods are presented. In particular, we considered the methods proposed in Campeau-Lecours et al. (2016) and Dimeas and Aspragathos (2016).

First of all, specific experiments have been performed in order to test the heuristic and how the adaptation is used to handle the oscillatory behavior. These specific experiments have been performed restricting robot motion to only one translational DOF, in order to obtain results that can be fairly compared with those presented in the mentioned references. The inertia and damping initial parameters have been set equal to $m(0) = 0.5\ kg$ and $d(0) = 5\ {}^{kg}/_{m^2}$, since these values have been found in Dimeas and Aspragathos (2016) to be the minimum stable admittance gains for a KUKA LWR

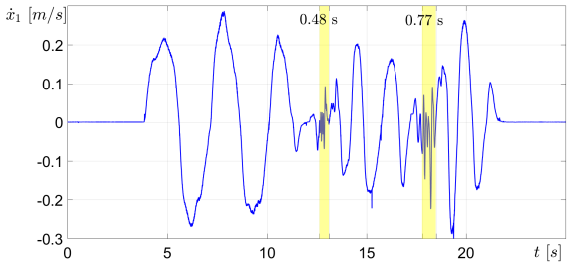

(a) Velocity of the robot along the considered translational DOF

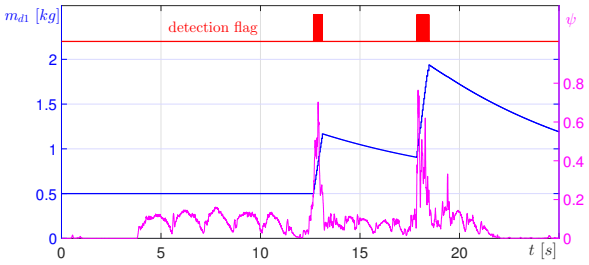

(b) Evolution over time of the detection index $\psi(t)$ (magenta line), and of the subsequent inertia adaptation (blue line). A detection flag (red line) is added to show when the heuristic detects that oscillations are rising.

Figure 10. Detection and adaptation of the rising oscillations using the proposed method.

4+, which is also the robot used in our experiments. In these conditions, the detection threshold has been properly tuned with the procedure defined in Section 4.3 and it resulted $\varepsilon = 0.22$. Whenever the user excessively stiffens his/her arm, high-frequency oscillations appear in the velocity of the robot (Figure 10(a)). Figure 10(b) shows, in magenta, the evolution over time of the detection index $\psi(t)$ as defined in (9). A boolean detection flag is depicted with a red line in Figure 10(b). As it can be seen, the rising oscillations are rightly detected and the inertia (blue line) is adapted accordingly. As shown in Figure 10(a), when an oscillating behavior arises (yellow regions), the adaptation of the parameters allows to stabilize the system $0.48\ s$ after the occurrence of the first oscillation and $0.68\ s$ after the occurrence of the second oscillation. Obviously, the

Table 4. Results of two-way ANOVA on user tests for the brushing task.
p-values lower than 0.05 (yellow cells) suggests that there is a relevant effect due to the related factor.

Setup		Time		Zero-crossings		Force RMS	
		mode	users	mode	users	mode	users
PUMA	p-value	0.091	**0.001**	**<0.001**	**0.002**	**<0.001**	**<0.001**
KUKA	p-value	**0.009**	**0.043**	0.232	0.314	0.361	**<0.001**

Table 5. Results of qualitative evaluations of the brusing task with QUEAD (Schmidtler et al. (2017)).

Setup	Usefulness	Ease of use	Emotions	Attitude	Comfort
PUMA	5.33	5.73	5.68	6.1	5.7
KUKA	5.5	5.85	5.61	5.83	6

difference in the adaptation times is due to the different attitude of the operator during the interaction, the different amplitude of the oscillations and, finally, to the starting values of the parameters when the adaptation is performed. However, thanks to the users study provided in Sections 6.1 and 6.2, we could verify that, from the user perspective, all the adaptation periods were sufficiently short amounts of time, since the adaptation of the parameters was achieved before the user could actually feel the rising oscillations.

Then, we performed similar experiments applying our implementation of the methods proposed in Campeau-Lecours et al. (2016) and Dimeas and Aspragathos (2016). The same The results of the comparison are analyzed in the remaining part of this section. As said, the experiments consider only one translational DOF and initial inertia and damping parameters set equal to $m(0) = 0.5\ kg$ and $d(0) = 5\ {}^{kg}/_{m^2}$ for all the compared methods. Moreover, the same experienced user performed all the interaction tests for this comparison, aiming to minimize the inherent variability on the conditions of the experiment due to the human behavior. An alternative solution to avoid such a variability could be the use of a variable stiffness apparatus emulating the average stiffness levels of a human arm, as suggested by Dimeas and Aspragathos (2016). Figure 11 shows the results of the implementation of the approach presented in Campeau-Lecours et al. (2016), based on the real-time computation of a vibration index, from minima and maxima detected on the robot velocity estimation, and the adaptation of admittance parameters by changing inertia and damping according to the vibration index. More precisely, if the vibration index is lower than a threshold $v.i._{min}$, the admittance parameters are set to their initial values $m(0)$ and $d(0)$; if the index exceeds an upper bound $v.i._{max}$, they are set to higher values, expected to guarantee a stable interaction (in our experiments, $10 \cdot m(0)$ and $10 \cdot d(0)$), and the parameters are changed from lower to higher values according to a linear function of the vibration index, during transient conditions. It is also important to remark that Campeau-Lecours et al. (2016) suggest the use of the vibration index to adapt also the gains of the inner robot motion controller, which is however not feasible in our setup. In particular, Figure 11(a) shows the velocity of the robot and the regions where oscillations arise (yellow regions), while

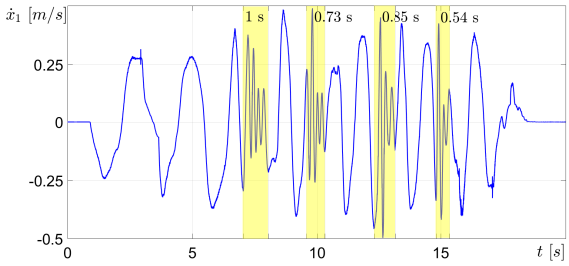

(a) Velocity of the robot along the considered translational DOF.

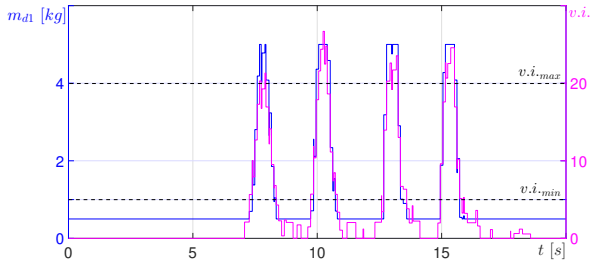

(b) Evolution over time of the variation index (magenta line) and of the inertia variation (blue line).

Figure 11. Detection and adaptation of the rising oscillations using the method proposed in Campeau-Lecours et al. (2016).

Figure 11(b) shows the evolution over time of the variation index (red line) and of the inertia variation (blue line). The paper Campeau-Lecours et al. (2016) provides guidelines to render the approach robust against the noise of the signal (i.e. by tuning a parameter called narrow time window). However, in practical implementations, a significant level of noise may require additional countermeasures to reduce its impact. Indeed, as shown in Figure 12, without additional signal filtering and a threshold-based logic to discard minima and maxima due to noise, the index becomes quite large even in absence of oscillations (e.g. in the time intervals $[7.8, 8.5]\ s$ and $[9.2, 9.9]\ s$). In these cases the index would be misleading in detecting the rising oscillations. Moreover, the method proposed in Campeau-Lecours et al. (2016) requires the tuning of two different time windows and two thresholds, to be performed empirically. In the method presented in

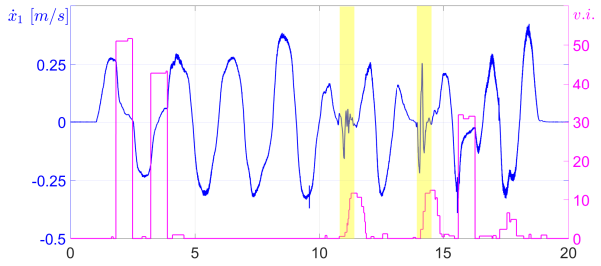

Figure 12. Evolution over time of the velocity of the robot (blue line) and of the variation index (red line) in case that no additional filtering or threshold-based noise mitigation solutions are included in the method proposed in Campeau-Lecours et al. (2016).

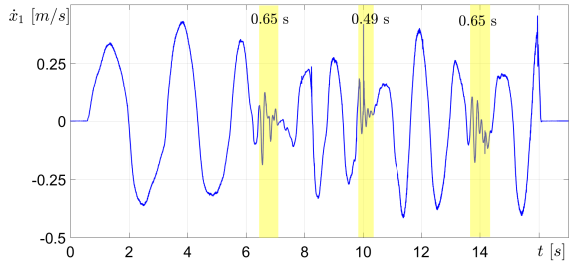

(a) Velocity of the robot along the considered translational DOF.

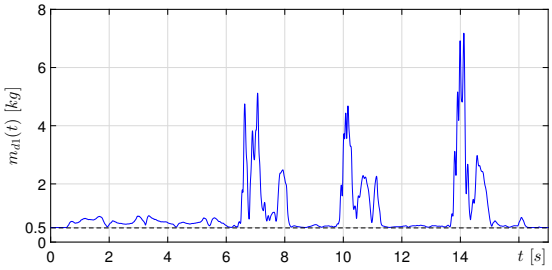

(b) Evolution over time of the inertia variation, given by the sum of the instability index and the initial inertia ($0.5\ kg$).

Figure 13. Detection and adaptation of the rising oscillations using the method proposed in Dimeas and Aspragathos (2016).

the current paper the detection threshold is automatically found by applying the procedure described in Section 4.3 and the detection index is not affected by noise, provided that a very simple debouncing logic is applied to avoid false positives. Figure 13 shows the results of the implementation of the approach presented in Dimeas and Aspragathos (2016), suggesting a peculiar formulation of a frequency-based instability index, which is then directly summed to the initial values of the admittance parameters. In particular, Figure 13(a) shows the velocity of the robot and the regions where oscillations arise (yellow regions), while Figure 13(b) shows the evolution over time of the inertia variation, that is given by the sum of the instability index and the initial inertia ($0.5\ kg$). The method presented in Dimeas and Aspragathos (2016) is not explicitly presented for the multi-DOF case. Indeed, the frequency-based instability index requires the calculation of the Fast Fourier Transform (FFT) on a moving time window, which can be computationally onerous if applied on multiple DOFs. Table 6 presents a comparison between the times required for computing the detection index during the experiments performed applying the three methods (i.e. the one proposed in this paper, the one presented in Campeau-Lecours et al. (2016) and the one presented in Dimeas and Aspragathos (2016)). The detection index proposed in this paper requires only the instantaneous computation of the norm defined in (9), while both the other approaches require to process time windows of several hundreds of samples. Moreover, the analysis is performed on the implementation for only one DOF. The time required by our proposed method is already calculated considering the multi-DOF case. On the other hand, an interesting aspect of the methods proposed in Campeau-Lecours et al. (2016) and Dimeas and Aspragathos (2016) is the fact that the admittance parameters are explicitly calculated according to the detection index, considering that high values of inertia and damping related to high values of the detection index inherently lead to reduce such a vibration/oscillation index. This relationship could also be taken into account, together with the passivity-preserving variation of the inertia, in the method proposed here.

7 Discussion and conclusion

Admittance control is a widely used approach for guaranteeing a compliant behavior of the robot in physical human-robot interaction. When an admittance-controlled robot is coupled with a human operator, the dynamics of the human can cause deviations from the desired behavior, that is the one imposed by the admittance control. The deviations result in high amplitude oscillations of the robot end-effector that may render the interaction with the robot unsafe for the user.

In this paper we presented a strategy for detecting the rising oscillations and adapting the parameters of the admittance control for restoring the stability. To detect the rising oscillations, a heuristic has been defined. A procedure for automatically tuning the detection threshold used in the heuristic has been proposed, by exploiting statistical methods. We then provided an algorithm for adapting the parameters of the admittance control when it is necessary, i.e. when a rising oscillation is detected, while preserving the passivity of the system. The parameters are gradually restored when the destabilizing factors are no longer active. An extensive validation has been performed on two robotic setups, with several users that performed two different tasks. The analysis of quantitative and qualitative results obtained during the experiments revealed that the proposed admittance adaptation strategy is capable of addressing the issue of rising oscillations in human-robot interactions with a minimal robot-dependent tuning, limited to those parameters strictly affected by the dynamic bounds of the robot. Other settings of the adaptation strategy are instead quite independent on the features of the robot. With regard to the dependency on the task, instead, it should be remarked that initial values of the inertia and damping matrices could be tuned according to the requirements of the task itself and, possibly, according to a user-specific selection. For example, allowing a user to practice the human-robot interaction for a longer time, with the only purpose of training the walk-through functionality for a given task, would probably allow

Table 6. Time required for computing the detection index $[\mu s]$.

Method	Mean value	Standard deviation	Min	Max
Proposed in this paper	17.46	0.46	16.81	59.62
Proposed in Campeau-Lecours et al. (2016)	458.03	10.25	426.76	571.37
Proposed in Dimeas and Aspragathos (2016)	206.39	6.30	197.02	273.40

to establish the admittance control parameter settings more comfortable for that user (i.e. less prone to generate rising oscillations because of the stiffness of his/her arm and his/her grasp on the robot end-effector). The forgetting factor for restoring the initial interaction model after an inertia augmentation is another parameter that could be user- and/or task-dependent.

However, these aspects were not investigated in this paper, whose objective is to present the passivity-preserving inertia adaptation strategy and a novel method for the tuning of the oscillation detection threshold.

Taking into consideration these issues is still an open problem. Together with the consideration of safety-related problems in industrial applications, solving these issues would lead to move a significant step towards implementation of the proposed strategy in a real industrial setup. Along these lines, the system can be rendered compliant with the international norms for collaborative robots (ISO 10218-1:2011, ISO 10218-2:2011, ISO/TS 15066:2016, Rosenstrauch and Kruger (2017)). Moreover, the proposed methodology can be integrated with other solutions as, e.g., the ones that render the admittance parameters explicitly dependent from the detection index.

References

Brys G, Hubert M and Struyf A (2004) A robust measure of skewness. *Journal of Computational and Graphical Statistics* 13(4): 996–1017.

Campeau-Lecours A, Otis M, Belzile P and Gosselin C (2016) A time–domain vibration observer and controller for physical human–robot interaction. *Mechatronics* 36: 45–53.

Chen H, He G, Xing J, Wang H and Chen L (2009) Pdf control of tracking error of robotic systems with any bounded stochastic disturbances. In: *Proceedings of the 4th IEEE Conference on Industrial Electronics and Applications*. pp. 1636–1641.

Colgate E and Hogan N (1989) The interaction of robots with passive environments: application to force feedback control. In: *Advanced Robotics*. Springer-Verlag.

De Stefano M, Artigas J and Secchi C (2017a) A passive integration strategy for rendering rotational rigid-body dynamics on a robotic simulator. In: *Proceedings of the IEEE/RSJ International Conference on Intelligent Robots and Systems*. pp. 2806–2812.

De Stefano M, Balachandran R, Artigas J and Secchi C (2017b) Reproducing physical dynamics with hardware-in-the-loop simulators: A passive and explicit discrete integrator. In: *Proceedings of the IEEE International Conference on Robotics and Automation*. pp. 5899–5906.

Dimeas F and Aspragathos N (2016) Online stability in human-robot cooperation with admittance control. *IEEE Transactions on Haptics* 9(2): 267–278.

Duchaine V and Gosselin C (2008) Investigation of human-robot interaction stability using lyapunov theory. In: *Proceedings of the IEEE International Conference on Robotics and Automation*. pp. 2189–2194.

Duchaine V, St-Onge BM, Gao D and Gosselin C (2012) Stable and intuitive control of an intelligent assist device. *IEEE Transactions on Haptics* 5(2): 148–159.

Eppinger S and Seering W (1986) On dynamic models of robot force control. In: *Proceedings of the IEEE International Conference on Robotics and Automation*.

Erden MS and Marić B (2011) Assisting manual welding with robot. *Robotics and Computer-Integrated Manufacturing* 27(4): 818–828.

Farsoni S, Talignani Landi C, Ferraguti F, Secchi C and Bonfè M (2017) Compensation of load dynamics for admittance controlled interactive industrial robots using a quaternion-based kalman filter. *IEEE Robotics and Automation Letters* 2(2): 672–679.

Ferraguti F, Preda N, Manurung A, Bonfè M, Lambercy O, Gassert R, Muradore R, Fiorini P and Secchi C (2015) An energy tank-based interactive control architecture for autonomous and teleoperated robotic surgery. *IEEE Transactions on Robotics* 31(5): 1073–1088.

Ferraguti F, Talignani Landi C, Secchi C, Fantuzzi C, Nolli M and Pesamosca M (2017) Walk-through programming for industrial applications. *Procedia Manufacturing* 11: 31–38.

Franken M, Stramigioli S, Misra S, Secchi C and Macchelli A (2011) Bilateral telemanipulation with time delays: A two-layer approach combining passivity and transparency. *IEEE Transactions on Robotics* 27(4): 741–756.

Gallagher W, Gao D and Ueda J (2014) Improved stability of haptic human–robot interfaces using measurement of human arm stiffness. *Advanced Robotics* 28(13): 869–882.

Gerelli O and Bianco CGL (2009) Nonlinear variable structure filter for the online trajectory scaling. *IEEE Transactions on Industrial Electronics* 56(10): 3921–3930.

Ginos B (2009) *Parameter Estimation for the Lognormal Distibution*. Master's Thesis, Brigham Young University.

Grafakos S, Dimeas F and Aspragathos N (2016) Variable admittance control in phri using emg-based arm muscles co-activation. In: *Proceedings of the IEEE International Conference on Systems, Man, and Cybernetics*. pp. 001900–001905.

Hannaford B and Ryu JH (2002) Time-domain passivity control of haptic interfaces. *IEEE Transactions on Robotics and Automation* 18(1): 1–10.

Hubert M and Vandervieren E (2008) An adjusted boxplot for skewed distributions. *Computational Statistics & Data Analysis* 52(12): 5186 – 5201.

Johnson N, Kotz S and Balakrishnan N (1995) *Continuous Univariate Distributions*, *Probability and Mathematical Statistics*, volume 1 and 2. 2nd edition. Wiley.

Lamy X, Colledani F, Geffard F, Measson Y and Morel G (2009) Achieving efficient and stable comanipulation through adaptation to changes in human arm impedance. In: *Proceedings of the IEEE International Conference on Robotics and Automation*. pp. 265–271.

Lecours A, Mayer-St-Onge B and Gosselin C (2012) Variable admittance control of a four-degree-of-freedom intelligent assist device. In: *Proceedings of the IEEE International Conference on Robotics and Automation*. Minnesota, USA.

Lee D and Huang K (2010) Passive-set-position-modulation framework for interactive robotic systems. *IEEE Transactions on Robotics* 26(2): 354–369.

Okunev V, Nierhoff T and Hirche S (2012) Human-preference-based control design: Adaptive robot admittance control for physical human-robot interaction. In: *Proceedings of the IEEE International Conference on Robot and Human Interactive Communication*. pp. 443–448.

Peer A and Buss M (2008) Robust stability analysis of bilateral teleoperation systems using admittance-type devices. In: *Proceedings of the SICE Annual Conference*. Tokyo, Japan.

Podobnik J and Munih M (2007) Haptic interaction stability with respect to grasp force. *IEEE Transactions on Systems, Man, and Cybernetics, Part C (Applications and Reviews)* 37(6): 1214–1222.

Ranatunga I, Lewis FL, Popa DO and Tousif SM (2017) Adaptive admittance control for human-robot interaction using model reference design and adaptive inverse filtering. *IEEE Transactions on Control Systems Technology* 25(1): 278–285.

Rosenstrauch MJ and Kruger J (2017) Safe human-robot-collaboration-introduction and experiment using iso/ts 15066. In: *Proceedings of the International Conference on Control, Automation and Robotics*.

Ryu D, Song JB, Kang S and Kim M (2008) Frequency domain stability observer and active damping control for stable haptic interaction. *IET Control Theory & Applications* 2(4): 261–268.

Schmidtler J, Bengler K, Dimeas F and Campeau-Lecours A (2017) A questionnaire for the evaluation of physical assistive devices (quead). In: *Proceedings of the IEEE International Conference on Systems, Man and Cybernetics*. Canada, pp. 876–881.

Secchi C, Stramigioli S and Fantuzzi C (2006) Position drift compensation in port-hamiltonian based telemanipulation. In: *Proceedings of the IEEE/RSJ International Conference on Intelligent Robots and Systems*. pp. 4211–4216.

Talignani Landi C, Ferraguti F, Sabattini L, Secchi C, Bonfè M and Fantuzzi C (2017a) Variable admittance control preventing undesired oscillating behaviors in physical human-robot interaction. In: *Proceedings of the IEEE International Conference on Intelligent Robots and Systems*. Vancouver, Canada.

Talignani Landi C, Ferraguti F, Sabattini L, Secchi C and Fantuzzi C (2017b) Admittance control parameter adaptation for physical human-robot interaction. In: *Proceedings of the IEEE International Conference on Robotics and Automation*. Singapore.

Talignani Landi C, Ferraguti F, Secchi C and Fantuzzi C (2016) Tool compensation in walk-through programming for admittance-controlled robots. In: *Proceedings of the Annual Conference of IEEE Industrial Electronics Society*. Firenze, Italy.

Tsumugiwa T, Yokogawa R and Hara K (2002) Variable impedance control based on estimation of human arm stiffness for human-robot cooperative calligraphic task. In: *Proceedings of the IEEE International Conference on Robotics and Automation*, volume 1. pp. 644–650.

Tsumugiwa T, Yokogawa R and Yoshida K (2004) Stability analysis for impedance control of robot for human-robot cooperative task system. In: *Proceedings of the IEEE/RSJ International Conference on Intelligent Robots and Systems*. Sendai, Japan.

Villani L and De Schutter J (2008) Force control. In: Siciliano B and Khatib O (eds.) *Springer Handbook of Robotics*, chapter 7. Springer Berlin Heidelberg.